Weather and Climate Extremes 10 (2015) 40–55

Contents lists available at ScienceDirect

Weather and Climate Extremes

journal homepage: www.elsevier.com/locate/wace

Assessment of temporal and spatial changes of future climate in the Jhelum river basin, Pakistan and India

Rashid Mahmood [a,c,*], Mukand S Babel [b], Shaofeng JIA [a,c]

[a] Department of Irrigation and Drainage, Faculty of Agricultural Engineering and Technology, University of Agriculture, Faisalabad, Pakistan
[b] Water Engineering and Management, Asian Institute of Technology, Pathumthani, Thailand
[c] Institute of Geographic Science and Natural Resources Research / Key Laboratory of Water Cycle and Related Land Surface Processes, Chinese Academy of Sciences, Beijing, 100101, China

ARTICLE INFO

Article history:
Received 26 October 2014
Received in revised form
20 July 2015
Accepted 27 July 2015
Available online 30 July 2015

Keywords:
Climate change
Downscaling
Statistical downscaling
Jhelum River basin
Pakistan
India
Temperature
Precipitation

ABSTRACT

The present study investigated future temporal and spatial changes in maximum temperature, minimum temperature, and precipitation in two sub-basins of the Jhelum River basin—the Two Peak Precipitation basin (TPPB) and the One Peak Precipitation basin (OPPB)—and in the Jhelum River basin on the whole, using the statistical downscaling model, SDSM. The Jhelum River is one of the biggest tributaries of the Indus River basin and the main source of water for Mangla reservoir, the second biggest reservoir in Pakistan.

An advanced interpolation method, kriging, was used to explore the spatial variations in the study area. Validation results showed a better relationship between simulated and observed monthly time series as well as between seasonal time series relative to daily time series, with an average R^2 of 0.92–0.97 for temperature and 0.22–0.62 for precipitation.

Mean annual temperature was projected to rise significantly in the entire basin under two emission scenarios of HadCM3 (A2 and B2). However, these changes in mean annual temperature were predicted to be higher in the TPPB than the OPPB. On the other hand, mean annual precipitation showed a distinct increase in the TPPB and a decrease in the OPPB under both scenarios.

In the case of seasonal changes, spring in the TPPB and autumn in the OPPB were projected to be the most affected seasons, with an average increase in temperature of 0.43–1.7 °C in both seasons relative to baseline period. Summer in the TPPB and autumn in the OPPB were projected to receive more precipitation, with an average increase of 4–9% in both seasons, and winter in the TPPB and spring in the OPPB were predicted to receive 2–11% less rainfall under both future scenarios, relative to the baseline period.

In the case of spatial changes, some patches of the basin showed a decrease in temperature but most areas of the basin showed an increase. During the 2020s (2011–2040), about half of the basin showed a decrease in precipitation. However, in the 2080s (2071–2099), most parts of the basin were projected to have decreased precipitation under both scenarios.

1. Introduction

The concentration of CO_2 and other greenhouse gases has been increasing dramatically since 1950, mostly because of industrialization (Gebremeskel et al., 2005). This increase has caused a global energy imbalance and has increased global warming. According to the Fifth Assessment Report of the Intergovernmental Panel on Climate Change (IPCC), global (land and ocean) mean surface temperature as calculated by a linear trend over the period 1880–2012, show a warming of 0.85 °C (0.65–1.06 °C). An alarming increase of 0.78 (0.72–0.85) °C has been observed for the period of 2003–2012 with respect to 1850–1900. Global mean surface temperatures is projected to increase by 0.3–1.7 °C, 1.1 to 2.6 °C, 1.4–3.1 °C, and 2.6–4.8 °C under RCP2.6, RCP4.5, RCP6.0 and RCP8.5, respectively, for 2081–2100 relative to 1986–2005 (IPCC, 2013).

This global warming can disturb the hydrological cycle of the world, and can pose problems for public health, industrial and municipal water demand, water energy exploitation, and the ecosystem (Chu et al., 2010; Zhang et al., 2011).

* Corresponding author at: Department of Irrigation and Drainage, Faculty of Agricultural Engineering and Technology, University of Agriculture, Faisalabad, Pakistan.
E-mail address: rashi1254@gmail.com (R. Mahmood).

http://dx.doi.org/10.1016/j.wace.2015.07.002

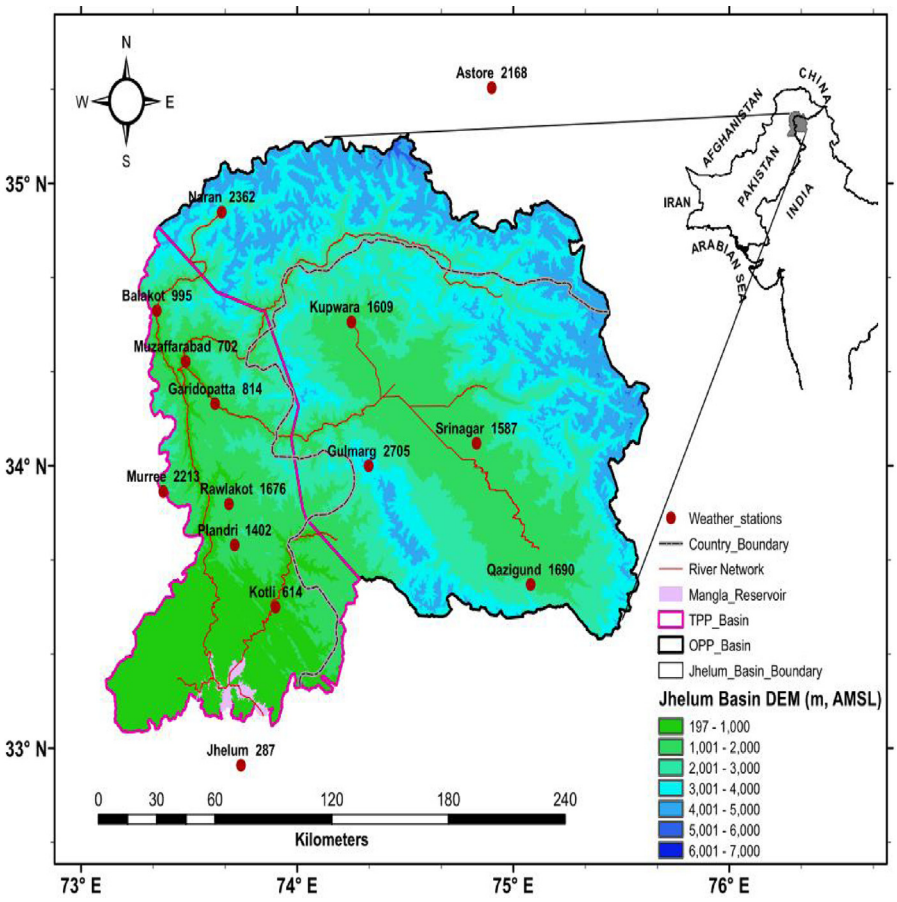

Fig. 1. Location map of the study area with the climate stations.

In the last few decades, Global Climate Models (GCMs)—the most advanced and numerical-based coupled models representing the global climate system—have been used to examine future changes in climate variables such as temperature, precipitation, and evaporation (Fowler et al., 2007). However, their outputs are temporally and spatially very coarse (Gebremeskel et al., 2005), which makes them useful only at continental and global levels. Their application at local/regional levels, such as at the basin and sub-basin scales, to assess the impacts of climate change on the environment and hydrological cycle, is problematic due to a clear resolution mismatch (Hay et al., 2000; Wilby et al., 2000). That is, GCMs cannot give a realistic presentation of local or regional scales due to parameterization limitations (Benestad et al., 2008). The local and regional scales are defined as 0–50 km and 50×50 km^2, respectively (Xu, 1999)

To overcome this problem, during the last two decades, many downscaling methods have been developed to make the large-scale outputs of GCMs useful at local/regional scales (Wetterhall et al., 2006). In the beginning, these methods were mostly implemented in Europe and in the USA but are now applied throughout the globe to examine changes in climate variables at the basin level (Mahmood and Babel, 2012).

Generally, downscaling techniques are divided into two main categories: Dynamical Downscaling (DD), and Statistical Downscaling (SD). In DD, a Regional Climate Model (RCM) of high resolution (5–50 km) (Chu et al., 2010), nested within a GCM, receives inputs from the GCM and then provides high resolution outputs on a local scale. Since the RCM is dependent on the boundary conditions of a GCM, there is a greater chance that systematic errors that belong to the driving fields of the GCM will be inherited by the RCM. In addition, simulations from RCMs are computationally intensive, and depend upon the domain size and resolution at which the RCMs are to run, which in turn limits the number of climate projections (Fowler et al., 2007).

In contrast, SD approaches, which establish a bridge among the large-scale variables (e.g., mean sea level pressure, temperature, zonal wind, and geopotential height) and local-scale variables (e.g., observed temperature and precipitation) by creating empirical/statistical relationships, are computationally inexpensive and much simpler than DD (Wetterhall et al., 2006). Moreover, SD approaches offer immediate solutions for downscaling climate variables and, accordingly, they have rapidly been adopted by a wider community of scientists (Wilby et al., 2000; Fowler et al., 2007). The limitation of SD is that historical meteorological station data over a long period of time is required to establish a suitable statistical or empirical relationship with large-scale variables (Chu et al., 2010). This relationship is considered to be temporally stationary, which is the main assumption of this method (Hay and Clark, 2003). In addition, SD is mainly dependent on the level of uncertainties of the parent GCM(s). DD, therefore, is a good alternative for SD in basins where no historical data is available (Benestad et al., 2008).

To date, many SD models have been developed for downscaling, and among them Statistical Downscaling Model (SDSM) was selected for this study. SDSM—a combination of multiple linear regression and a stochastic weather generator—is a well-known statistical model, and is frequently used for downscaling important climate variables (e.g., temperature, precipitation, and evaporation). The downscaled variables are used to assess hydrological responses under changing climatic conditions (Diaz-Nieto and Wilby, 2005; Gagnon et al., 2005; Gebremeskel et al., 2005; Wilby et al., 2006). SDSM has been widely used throughout the

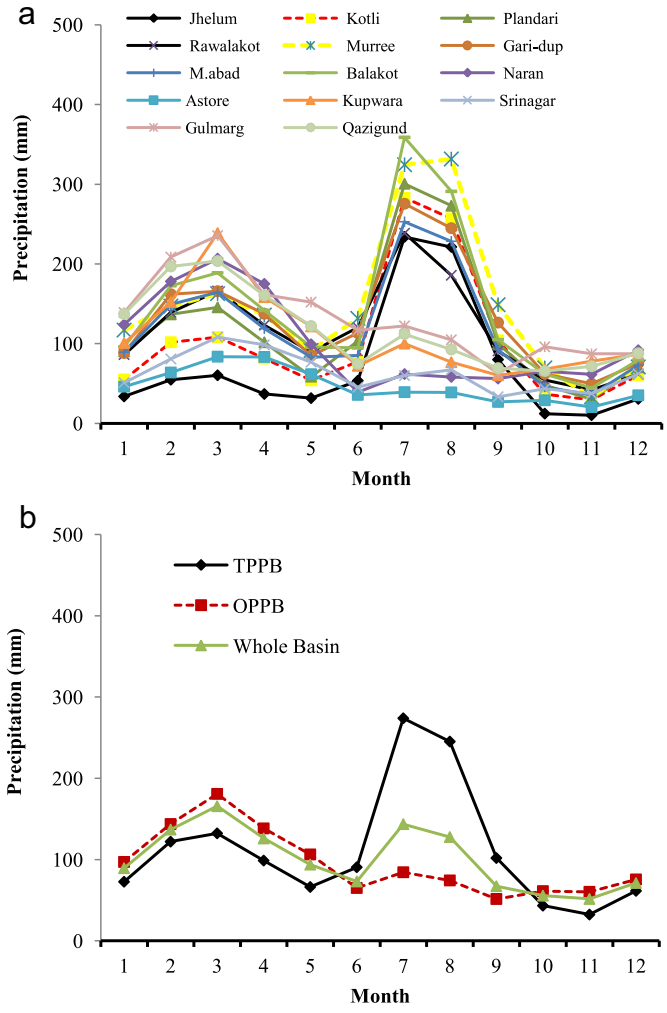

Fig. 2. Distribution of mean monthly rainfall at (a) all the weather stations and (b) in the TPPB, OPPB, and the whole Jhelum basin for 1961–1990 (the baseline period).

Table 1
Statistics of climate stations for the period of 1961-1990 in the Jhelum River basin.

	Station	Elevation	Annual precipitation (mm)	Mean T_{max} (°C)	Mean T_{min} (°C)	T_{mean} (°C)
	TPPB					
1	Jhelum	287	860	30.51	16.54	23.53
2	Kotli	614	1249	28.41	15.75	22.08
3	Plandri	1402	1459	22.73	11.30	17.01
4	Rawalakot	1676	1398	21.87	10.25	16.06
5	Murree	2213	1765	16.57	8.97	12.77
6	Garidopatta	814	1586	26.06	12.58	19.32
7	Muzaffarabad	702	1418	27.34	13.54	20.44
8	Balakot	995	1731	25.04	12.01	18.53
	Average	**1088**	**1341**	**26.21**	**13.50**	**19.85**
	OPPB					
9	Naran	2362	1217	11.14	1.15	6.14
10	Kupwara	1609	1314	19.64	6.30	12.93
11	Gulmarg	2705	1574	11.73	1.98	6.81
12	Srinagar	1587	764	19.76	7.37	13.52
13	Qazigund	1690	1395	19.11	6.57	12.80
14	Astore	2168	564	15.48	4.06	9.77
	Average	**2020**	**1139**	**16.88**	**5.04**	**10.93**
	Whole basin	**1487**	**1202**	**19.79**	**7.68**	**13.72**

T_{mean}=mean temperature, T_{max}=maximum temperature, T_{min}=minimum temperature

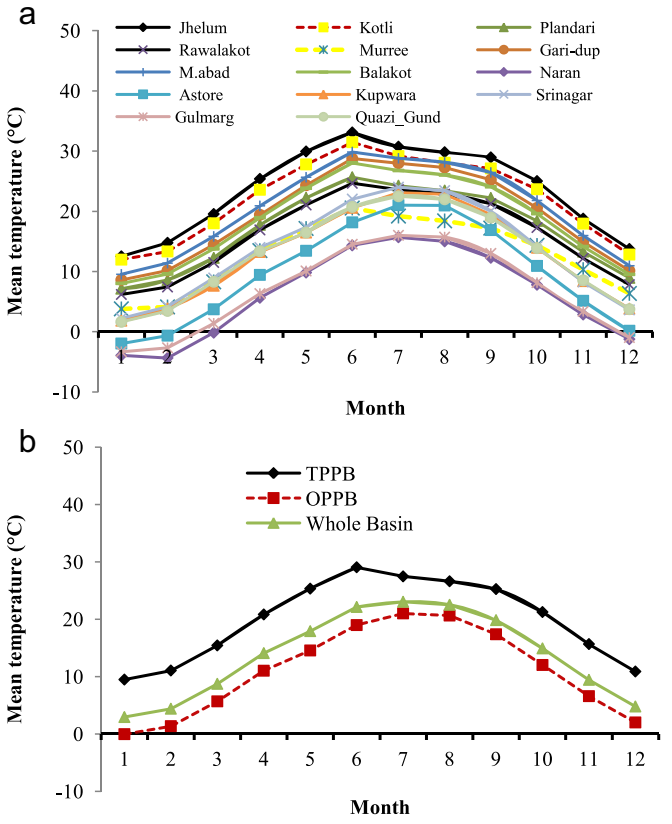

Fig. 3. Distribution of mean monthly temperature at (a) all the weather stations (b) in the TPPB, OPPB, and the entire Jhelum basin for 1961–1990 (the baseline period).

world in many impact assessment studies (Huang et al., 2011).

Several studies (Tripathi et al., 2006; Anandhi et al., 2007; Akhtar et al., 2008; Ghosh and Mujumdar, 2008; Mujumdar and Ghosh, 2008; Akhtar et al., 2009; Ashiq et al., 2010; Goyal and Ojha, 2010; Opitz-Stapleton and Gangopadhyay, 2010) have used SD and DD techniques in South Asia. However, most of these studies have been conducted in Indian river basins. A couple of studies, such as by Akhtar et al. (2008, 2009) and by Ashiq et al. (2010) using DD, and a study by Mahmood and Babel (2012) using SD, were conducted in Pakistan to investigate future changes in climate variables. In the study by Akhtar et al. (2008), a Regional Climate model, Providing Regional Climate for Impact Studies (PRECIS), and delta change were used to downscale mean temperature and precipitation in order to analyze hydrological responses to climate change in the Hindukush–Karakorum–Himalayas (HKH). However, future changes were only investigated under the A2 scenario and only for the period of 2071–2100. The study concluded that the simulations from PRECIS have several uncertainty sources. Ashiq et al. (2010) interpolated monthly precipitation outputs of PRECIS, run by Akhtar et al. (2008), from a coarse resolution (50×50 km^2) to a fine one (250×250 m^2) using some interpolation methods. Their study was carried out in the northwest region of the Himalayan Mountains and in the upper Indus plains of Pakistan. They also covered a small part of the Jhelum River basin, located inside Pakistan. The study's conclusion was that systematic errors associated with an RCM cannot be reduced by a simple interpolation methods.

Mahmood and Babel (2012) evaluated two sub-models of SDSM (annual and monthly sub-models) out of three sub-models (monthly, annual, and seasonal) in the Jhelum River basin. They concluded that the annual sub-model cannot be used to investigate the intra-annual (monthly or seasonal time series)

Table 2
NCEP predictors used in the screening process of SDSM.

Predictors		Description	Predictors		Description
1	p_f	Surface airflow strength	14	r500	500 hPa relative humidity
2	p_u	Surface zonal velocity	15	p8_f	850 hPa airflow strength
3	p_v	Surface meridional velocity	16	p8_u	850 hPa zonal velocity
4	p_z	Surface vorticity	17	p8_v	850 hPa meridional velocity
5	p_th	Surface wind direction	18	p8_z	850 hPa vorticity
6	p_zh	Surface divergence	19	p8th	850 hPa wind direction
7	rhum	Surface relative humidity	20	p8zh	850 hPa divergence
8	p5_f	500 hPa airflow strength	21	r850	850 hPa relative humidity
9	p5_u	500 hPa zonal velocity	22	p500	500 hPa geopotential height
10	p5_v	500 hPa meridional velocity	23	p850	850 hPa geopotential height
11	p5_z	500 hPa vorticity	24	temp	Mean temperature at 2 m height
12	p5th	500 hPa wind direction	25	shum	Surface specific humidity
13	p5zh	500 hPa divergence	26	mslp	Mean sea level pressure

Table 3
Selected predictors and their mean absolute partial correlation coefficients during the screening process of SDSM.

	Tmax	Abs P.r	Tmin	Abs P.r	Precipitation	Abs P.r
TPPB	**temp**	0.73	**temp**	0.82	**Shum**	0.21
	r500	0.22	rhum	0.18	p5_v	0.14
	P8_z	0.19	r500	0.12	r850	0.10
			P8_z	0.32	p8_v	0.15
					Mslp	0.12
OPPB	**temp**	0.76	**temp**	0.79	**p5_v**	0.23
	p_u	0.38	p_u	0.37	p8_v	0.14
	p_z	0.32	p_z	0.32	p5_z	0.11
	P8_z	0.25	p8_z	0.26	p8_z	0.08
	r500	0.17				

Words in bold are super predictors; *Abs P.r* is the absolute partial correlation coefficient

variations in climate variables (like temperature and precipitation) without Bias Correction, although SDSM was able to predict mean annual values quite well. They also concluded that the monthly sub-model is capable of examining intra-annual variations without any Bias Correction.

No studies, to the best of our knowledge, have investigated the temporal and spatial future changes in maximum temperature, minimum temperature, and precipitation under A2 and B2 scenarios in the upper Jhelum River basin—one of the biggest tributaries of the Indus River basin and drains entirely into Mangla reservoir, the second biggest reservoir in Pakistan.

In the present study, the monthly sub-model of SDSM, as recommended by Mahmood and Babel (2012), was applied to analyze the temporal and spatial changes in maximum temperature, minimum temperature, and precipitation for the period of 2011–2099, under A2 and B2 scenarios of HadCM3. Since the study area is mountainous and has great altitudinal variations as shown in Fig. 1, an advanced spatial interpolation method, Kriging, was used to explore the spatial variability in the basin. For the sake of detailed analysis, the whole Jhelum basin was divided into two sub-basins, based on precipitation regimes. This study can be a guide for researchers who wish to apply statistical downscaling methods on mountainous regions in the Upper Indus basin, which is highly influenced by the monsoons.

2. Study area and data description

2.1. Study area

The upper Jhelum River basin—located in Pakistan and India—stretches between 73–75.62 °E and 33–35 °N, as shown in Fig. 1. The Jhelum River, the second biggest tributary of the Indus River system (Ahmad and Chaudhry, 1988), has a drainage area of 33,342 km^2, with an elevation ranging from 235 to 6285 m. The whole basin drains into Mangla Reservoir, constructed in 1967, which is the second biggest reservoir in Pakistan. The main purpose of this dam is to provide irrigation water to 6 million hectares of land. Its secondary function is to produce hydropower; it has an installed capacity of 1000 MW, contributing 6% of the country's installed capacity (Archer and Fowler, 2008; Qamer et al., 2008). For the purposes of the present study, the basin was divided into

Table 4
Validation (1991-2000) of SDSM for Tmax, using daily, monthly, and seasonal time series in the Jhelum River basin.

		R (%)		R^2 (%)		*RMSE* (°C)		μ (°C)	
		Range	Mean	Range	Mean	Range	Mean	Range	Mean
Daily	Obs							10.2–30.41	21.04
	NCEP	84–92	87.48	71–85	76.5	3.08–3.98	3.52	11.5–30.55	21.02
Monthly	Obs							10.12–30.01	21.00
	NCEP	95–98	96.48	89–97	93.1	1.55–2.41	1.88	11.47–30.52	20.98
	A2	94–98	95.96	88–96	92.1	1.70–3.33	2.12	11.29–30.49	21.09
	B2	93–98	00.96	89–96	92.0	1.73–3.25	2.17	11.32–30.52	21.16
Seasonal	Obs							10.12–30.01	21.00
	NCEP	96–99	97.67	92-98	95.4	1.06–2.04	1.40	11.47–30.52	20.99
	A2	95–99	97.65	92-98	95.3	1.11–2.75	1.47	11.29–30.49	21.09
	B2	95–99	00.97	91-98	94.6	1.22–2.74	1.59	11.32–30.52	21.16

R=Correlation coefficient, R^2=Coefficient of determination, *RMSE*=Root mean square error, and μ=mean

Table 5
Validation (1991–2000) of SDSM for T_{min}, using daily, monthly, and seasonal time series in the Jhelum River basin.

		R (%)		R^2 (%)		*RMSE* (°C)		μ (°C)	
		Range	Mean	Range	Mean	Range	Mean	Range	Mean
Daily	Obs							1.54–16.85	9.15
	NCP	88–95	92.27	77–89	85.2	2.32–3.26	2.642	1.18–16.51	8.98
Monthly	Obs							1.48–16.82	9.11
	NCEP	93–99	97.49	87–98	95.1	1.09–2.41	1.45	1.13–16.47	8.94
	A2	93–98	96.81	86–97	93.7	1.23–3.15	1.75	1.08–16.51	9.05
	B2	93–98	96.59	86–97	93.3	1.26–3.16	1.82	1.10–16.52	9.06
Seasonal	Obs							1.48–16.82	9.11
	NCEP	95–99	98.37	90–99	96.8	0.56–2.00	1.045	1.13–16.47	8.94
	A2	94–99	98.20	89–99	96.4	0.60–2.50	1.182	1.08–16.51	9.05
	B2	94–99	97.90	88–99	95.9	0.63–2.58	1.268	1.10–16.52	9.06

R=Correlation coefficient, R^2=Coefficient of determination, *RMSE*=Root mean square error, and μ=mean

Table 6
Validation (1991–2000) of SDSM for precipitation, using daily, monthly, and seasonal time series in the Jhelum River basin.

		R (%)		R^2 (%)		*RMSE* (mm)		μ (mm)	
		Range	Mean	Range	Mean	Range	Mean	Range	Mean
Daily	Obs							1.74–5.69	3.92
	NCEP	10–39	25.045	8–15	9.6	1.9–5.5	3.65	1.69–5.53	3.62
Monthly	Obs							53–174	119.77
	NCEP	43–85	62.70	21–73	42.0	24–82	50.67	50–166	110.41
	A2	29–72	51.40	18–51	28.1	43–12	86.64	50–154	109.87
	B2	25–68	43.91	13–46	22.3	47–13	89.89	48–149	105.13
Seasonal	Obs							53–174	119.30
	NCEP	50–93	70.90	25-87	61.7	17–55	35.40	50–165	110.21
	A2	40–81	66.00	30–67	55.2	27–85	53.71	50–154	109.87
	B2	26–77	55.27	22–60	50.8	33–95	57.88	48–149	105.13

R=Correlation coefficient, R^2=Coefficient of determination, *RMSE*=Root mean square error, and μ=mean

two parts, based on the precipitation regimes of the basin, as discussed in Section 2.3.

2.2. Data description

Historical daily data of maximum temperature (Tmax), minimum temperature (Tmin), and precipitation (P) was collected from the Water and Power Development Authority of Pakistan (WAPDA), Pakistan Meteorological Department (PMD), and the Indian Meteorological Department (IMD). The dataset was obtained from 14 climate stations located in the basin (Fig. 1) for the period of 1961–2000. The historical data of Kupwara, Srinagar, Gulmarg, and Qazigund was obtained from the IMD; the data of Rawlakot, Plandri, Kotli, and Naran was obtained from the WAPDA; and, the data of Muzaffarabad, Jhelum, Garidopatta, Balakot, Murree, and Astore was obtained from PMD. Some part of the daily P data for Srinagar and Qazigund for the period of 1961–1970 was acquired from the National Climate Data Center (NCDC). Although Astore and Jhelum do not lie in the upper Jhelum River basin, these stations were included in the present study due to the lack of climate stations in the basin. In addition, both stations have good quality historical meteorological data. There were some missing values on some weather stations which was filled by multiple imputation method, using winMice software (Jacobusse, 2005)

The daily predictors of National Centers for Environmental Prediction (NCEP) for 1961–2001 and the daily predictors of HadCM3 (A2 and B2 scenarios) for 1961–2099 were collected from a Canadian website (http://www.cccsn.ec.gc.ca/?page=dst-sdi). A2 and B2 are the IPCC emission scenarios of HadCM3 and are mostly used for regional impact assessment studies. These predictors are specially prepared for SDSM. During the preparation, the NCEP predictors (2.5° × 2.5°) were first interpolated to the grid resolution of HadCM3 (2.5° × 3.75°) to eliminate any spatial mismatch. Then, the NCEP and HadCM3 predictors were normalized with mean and standard deviations of a long period (1961–1990) (CCCSN, 2012).

2.3. Climatic condition in the study area

The mean monthly rainfall regimes of all the climate stations used in this study for the period of 1961–1990 are shown in Fig. 2 (a). Naran, Srinagar, Kupwara, Gulmarg, Astore and Qazigund climate stations experience one big peak in March, and Kotli, Jhelum, Murree, Plandri, Rawlakot, Murree, Garidopatta, Muzaffarabad and Balakot experience two peaks, one small peak around March, and other big peak around July. According to the P regimes, the whole basin was divided into two sub-basins: (1) the One Peak Precipitation basin (OPPB), and (2) the Two Peak Precipitation basin (TPPB). The OPPB contains most of the northeast parts of the Jhelum basin, including Srinagar, Gulmarg, Qazigund and Astore weather stations, and some of the northwest parts of the basin, including Naran and Kupwara weather stations. The TPPB consists of the southwest parts of the basin, containing Jhelum, Kotli, Plandri, Rawlakot and Murree climate stations, and the northwest

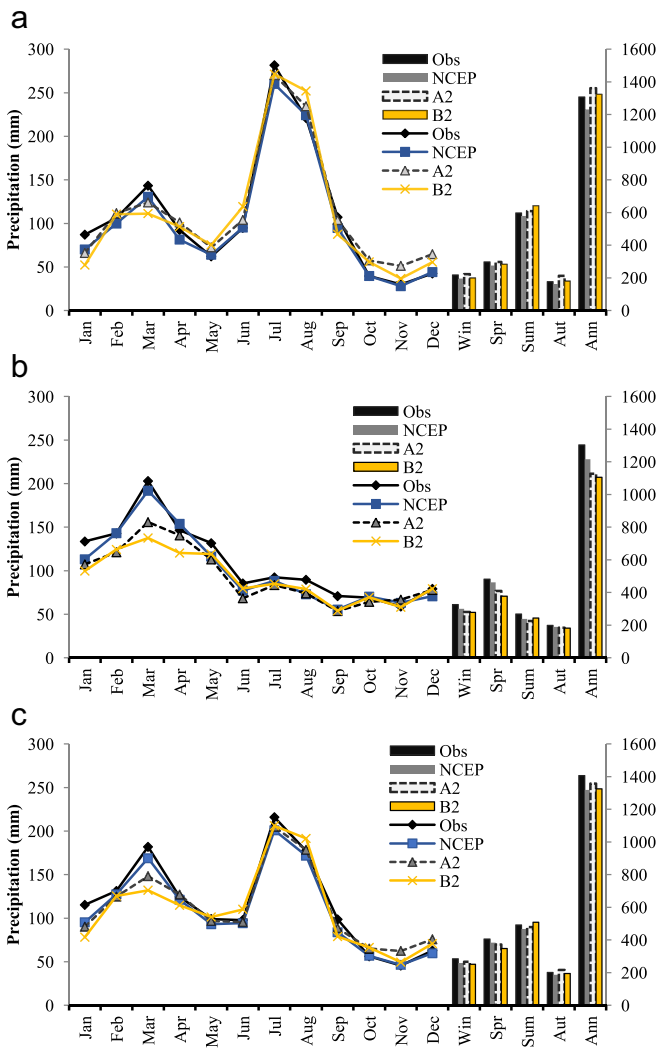

Fig. 4. Observed versus simulated precipitation in the (a) TPPB, (b) OPPB, (c) whole Jhelum basin, for the validation (1991–2000) of SDSM. *Win, Spr, Sum, Aut and Ann* describe winter (December–February), spring (March–May), summer (June–August), autumn (September–November), and annual (January–December), respectively.

part of the basin that has climate stations like Garidopatta, Muzaffarabad, and Balakot. The locations of these stations are shown in Fig. 1. The one big peak (July) in the basin is the result of summer monsoon (June–July–August), which occurs due to the saturated south western winds from the Bay of Bengal and Arabian Sea. The second small peak (March) is the result of the Western disturbances (WDs) system in winter. Generally the whole Pakistan and particularly its northwestern pats receive precipitation due to the WDs. The WDs are natured by the depression over the Mediterranean regions that take precipitation to central southwest Asia in the months of December–March (Ahmad et al., 2015). More details about the Summer Monsoon and WDs are described in Ahmad et al. (2015).

Fig. 2 and Table 1 illustrate that the TPPB, with a mean annual P of 1341 mm, is relatively wetter than the OPPB, which has a mean annual P of 1139 mm. A mean annual P of 1202 occurs in the basin as a whole. July and March are the wettest months in the TPPB and OPPB respectively, and November and September are the driest months in the TPPB and OPPB respectively. As for climate stations, Murree (with a mean annual P of 1765 mm) and Kotli (with a mean annual P of 1249 mm) are the wettest and driest weather stations, respectively, inside the TPPB, and Balakot (1731 mm) and Srinagar (764 mm) are the wettest and driest climate stations, respectively, in the OPPB.

Fig. 3 and Table 1 show that the TPPB is hotter than the OPPB, with mean temperatures of 19.85 °C in the former and 10.93 °C in the latter. The whole basin has a mean temperature of 13.72 °C. The hottest month is June in the TPPB and July in the OPPB as well as in the whole basin. January is the coldest month in both sub-basins. As for climate stations, Kotli (with a mean temperature of 22 °C) and Naran (with a mean temperature of 6.14 °C) are the hottest and coldest stations, respectively, in the study area.

3. Methodology

3.1. Description of SDSM

SDSM is a combination of the Stochastic Weather Generator (SWG) and Multiple Linear Regression (MLR). In MLR, statistical/empirical relationships between NCEP predictors and predictands are established, which leads to the production of some regression parameters. These regression parameters, along with NCEP or GCM predictors, are then used by SWG to generate a daily time series (Wilby et al., 2002; Liu et al., 2009).

In SDSM, a combination of different indicators such as the correlation matrix, partial correlation, *P* value, histograms, and scatter plots can be used to select some suitable predictors through a multiple linear regression model. Multiple co-linearity, or the correlations between the predictors, must be considered during the selection of predictors. This can mislead during calibration of model. For example, if there is high co-linearity among the predictors during the calibration, there will be high value of coefficient of determination (R^2). This high value of R^2 can be due to co-linearity not due to correlation between predictand and predictors. Ordinary Least Squares (OLS) and Dual Simplex (DS) are two optimization methods. OLS was selected for this study, which is faster than DS and produces results comparable with DS (Huang et al., 2011). Three kinds of sub-models—monthly, seasonal, and annual—are available in SDSM to establish statistical/empirical relationships between predictands and predictors. In the monthly sub-model, 12 regression equations are developed—one for each month—during the calibration process. SDSM has two kinds of sub-models: conditional and unconditional. The conditional sub-model is used for dependent variables such as P and evaporation, and the unconditional sub-model is used for independent variables such as temperature during calibration (Wilby et al., 2002; Chu et al., 2010; Mahmood and Babel, 2012).

Unlike temperature, P data is usually not normally distributed. So, P data is made normal by SDSM before it is used in regression equations (Khan et al., 2006). For example, Khan et al. (2006), Huang et al. (2011), and Mahmood and Babel (2012) have used the fourth root to turn P data into normal before using it in a regression equation. For the development of SDSM, two kinds of daily time series, observed and NCEP, are required. SDSM simulates daily time series as outputs, forcing NCEP or HadCM3 predictors (Huang et al., 2011). A full mathematical detail is presented in (Wilby et al., 1999).

3.2. Selection of predictors

In statistical downscaling techniques, the first and most important process is the screening of large-scale variables (Wilby et al., 2002; Huang et al., 2011). Four main indicators—explained variance, the correlation matrix, partial correlation, and *P* value—are used during the selection of predictors in SDSM. A combination of partial correlation and *P* value is generally used for the screening process, as it has been in studies like (Wilby et al., 2002;

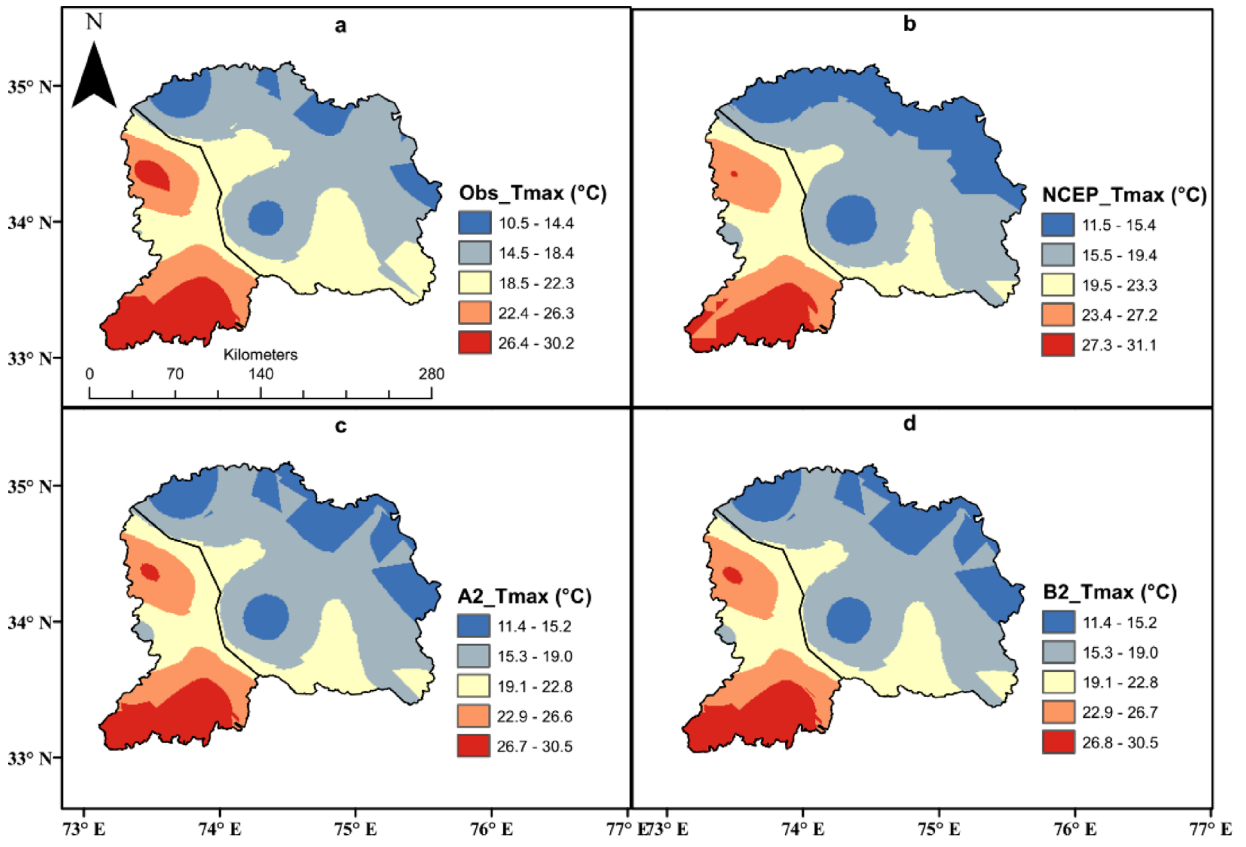

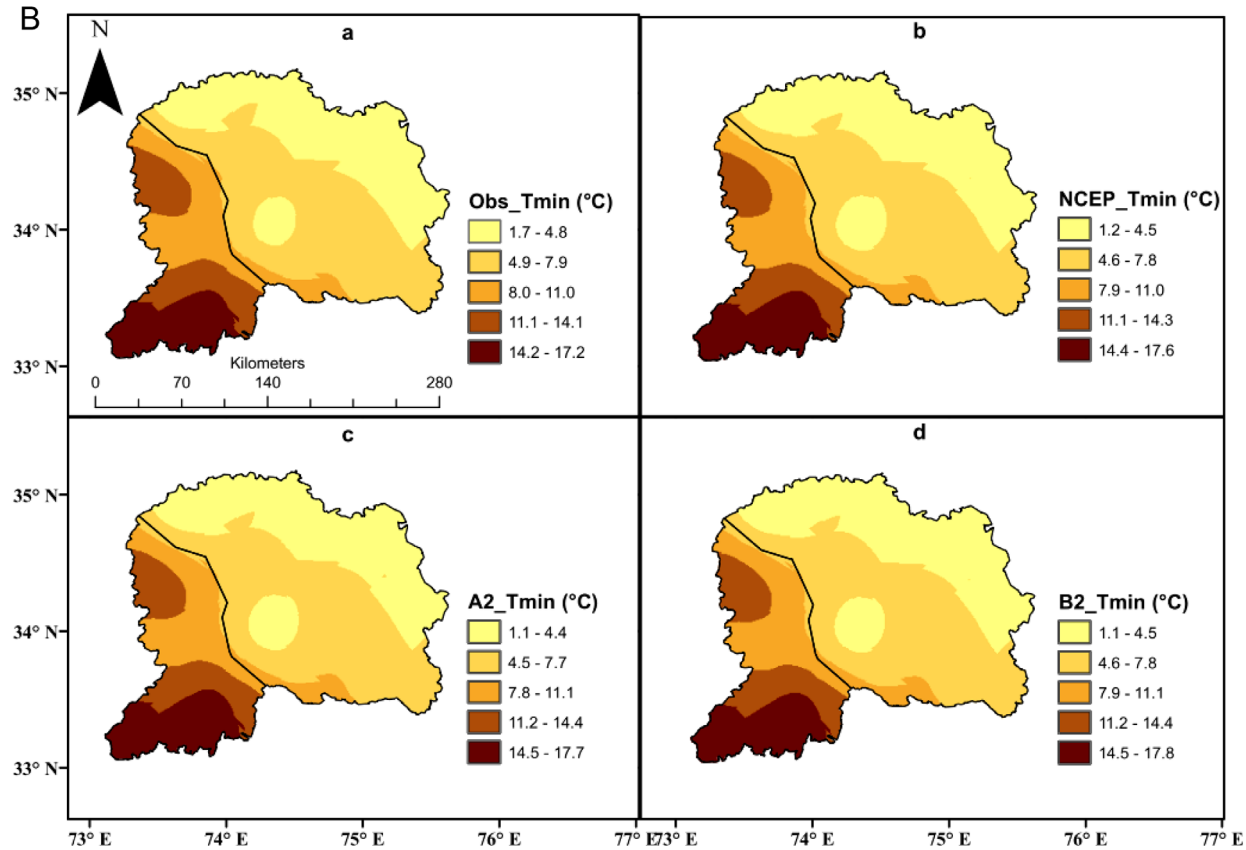

Fig. 5. Spatial distributions of observed versus simulated (A) T_{max}, (B) T_{min}, and (C) Precipitation for the validation (1991–2000) of SDSM in the Jhelum River basin.

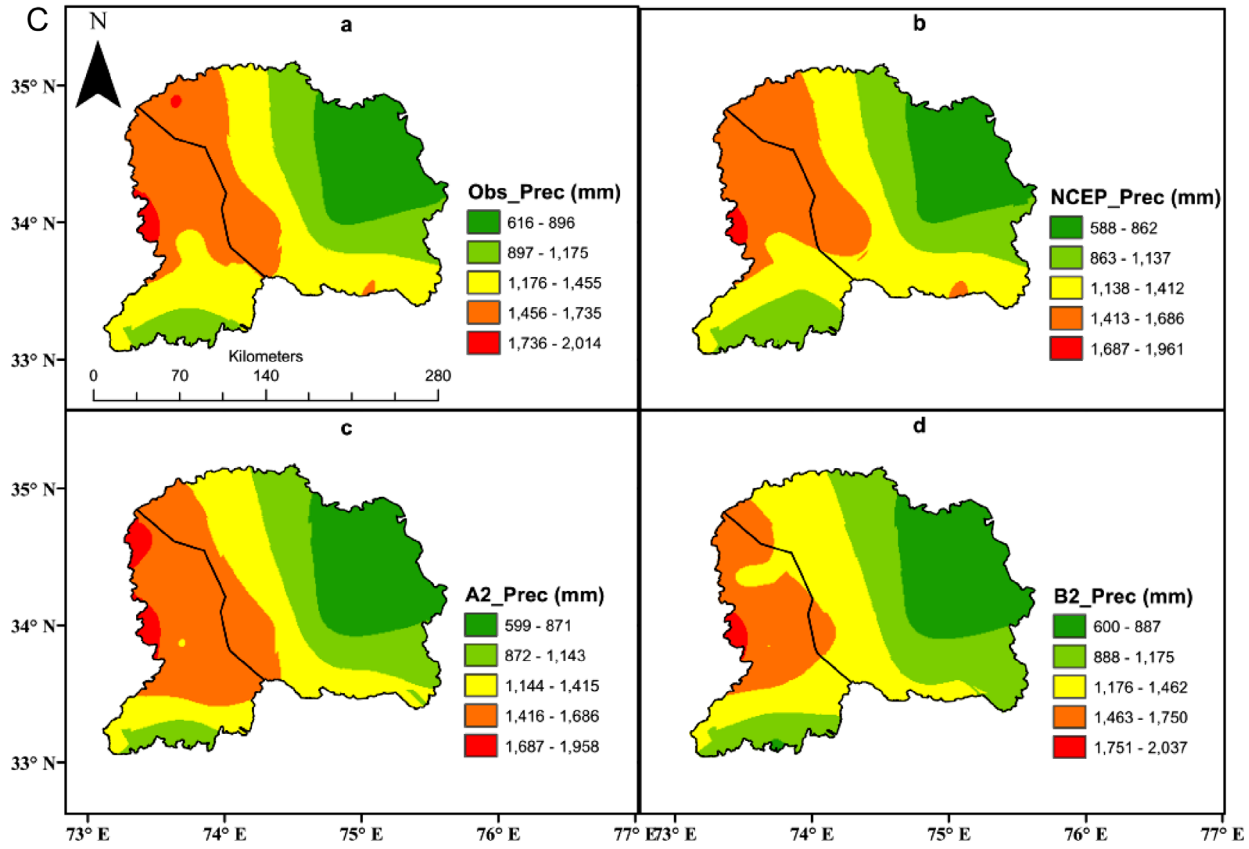

Fig. 5. (*continued*)

Table 7
AME and RMSSE between measured and predicted T_{max}, T_{min}, and Precipitation for the period of 1991–2000, during kriging interpolation, in the Jhelum River basin.

	Obs	NCEP	A2	B2
T_{min}				
AME (°C)	0.012	0.022	0.011	0.016
RMSSE	0.990	1.030	1.050	1.040
T_{max}				
AME(°C)	0.022	0.023	0.018	0.019
RMSSE	0.840	0.920	0.940	0.950
Precipitation				
AME(°C)	7.300	11.600	7.200	7.900
RMSSE	1.150	1.100	1.200	1.160

AME=Absolute Mean Error, RMSSE=Root Mean Square Standardized Error

Chu et al., 2010; Hashmi et al., 2011; Huang et al., 2011; Souvignet and Heinrich, 2011). The selection of predictors is more subjective and depends on the user's judgment. The main points, which must be considered during the selection of predictors, are multiple co-linearity among the predictors. In SDSM, the selection of the first and most prominent predictor is relatively easy and can be done with a simple correlation matrix. However, the selection of the second, third, fourth predictor and so on is more subjective. Therefore, in this study, a quantitative procedure used by Mahmood and Babel (2012) was applied for screening the predictors. In this procedure, a combination of the correlation matrix, partial correlation, *P* value, and percentage reduction in partial correlation was used. A set of 26 NCEP predictors, as described in Table 2, was regressed against each of predictands (T_{max}, T_{min}, and *P*) and some suitable predictors were screened out for calibration process. Multiple co-linearity was highly considered during screening process.

3.3. Calibration and validation

According to the available data, three data sets of periods 1961–1990, 1969–1990, and 1970–1990 were used for calibration, and a dataset from the period 1991–2000 for the validation of SDSM in this study. The monthly sub-model was used during calibration, utilizing the selected NCEP predictors for each of the predictands (T_{max}, T_{min}, and *P*), at each site. The unconditional sub-model was used for temperature without any transformation, and the conditional sub-model was set for P with fourth root transformation, before using it in regression equations. To check the performance of SDSM during calibration, two statistical indicators—the percentage of explained variance and standard error—were used in the present study, as they also have been in studies like Huang et al. (2011) and Wilby et al. (2002).

3.3.1. Temporal

For validation, Tmax, Tmin, and P datasets were simulated using NCEP, A2, and B2 predictors for 1991–2000. These simulated datasets were compared with observed datasets by calculating the correlation coefficient (*R*), the coefficient of determination (R^2), the root mean square error (RMSE), and the mean (μ). These indicators were first calculated for each weather station, and then, mean values were calculated from all the weather stations. The simulated data was also compared graphically with observed data to examine the variations in observed data captured by simulated data (Chu et al., 2010; Huang et al., 2011).

3.3.2. Spatial

SDSM was also validated by comparing the spatial distribution of mean annual observed data with simulated data. For this purpose, spatial maps for each variable (T_{max}, T_{min}, and *P*) were built by converting the mean annual point data into raster data by the

Kriging method, using ArcGis 9.3.

3.4. Description of Kriging method

Kriging is an advanced, computationally intensive, geostatistical interpolation method (Buytaert et al., 2006) that takes care not only the distance but also the degree of variation among known data points when estimating values in unknown areas. The first step in kriging interpolation is to inspect the data in order to identify the spatial structure, using empirical semivariogram or covariance. A semivariogram is a diagram that represents the connection between the distance (the distance between all the pairs of available data points) and semivariance, and covariance, in statistics, shows the strength of the correlation between two or more random variables. A basic principle on which the semivariogram bases is the points (stations, things etc.) closer to each other are more alike than the points that are farther apart.

The next step is to compute the weights for points from the model variogram. These weights are based on the distance between the observed (measured) points and the prediction points, and also on the overall spatial relationships among the measured values surrounding the prediction location. In kriging, different statistical indicators such as Absolute Mean Error (AME), Root Mean Square Error (RMSE), Average Standard Error (ASE) and Root Mean Square Standardized Error (RMSSE) etc. and different graphs such as graph between predicted and measured values, error graph and QQ-plot are used to check the performance of model (Pokhrel et al., 2013). Mathematical equations of these indicators are described in (Dai et al., 2014). In the present study, AME and RMSSE were used to check the performance of model. RMSSE is the ratio of RMSE to ASE. RMSSE and AME should be close to 1 and 0 respectively for satisfactory results. After satisfactory model performance, finally the maps were created for the study area. Mathematical detail about kriging method is described in Pokhrel et al. (2013).

3.5. Future changes

After satisfactory calibration and validation, Tmax, Tmin, and P data was simulated for three spells—the 2020s (2011–2040), the 2050s (2041–2070), and the 2080s (2071–2099). The datasets of each of these periods were compared to a baseline period to analyze future changes in the basin. In this study, the period from 1961 to 1990 was taken as the baseline period because this period has been used in the majority of climate change studies across the world (Huang et al., 2011). A 30-year period is also considered long enough to define local climate because it is likely to include dry, wet, cool, and warm periods. The IPCC also recommends such a length (of 30 years) for the baseline period (Gebremeskel et al., 2005).

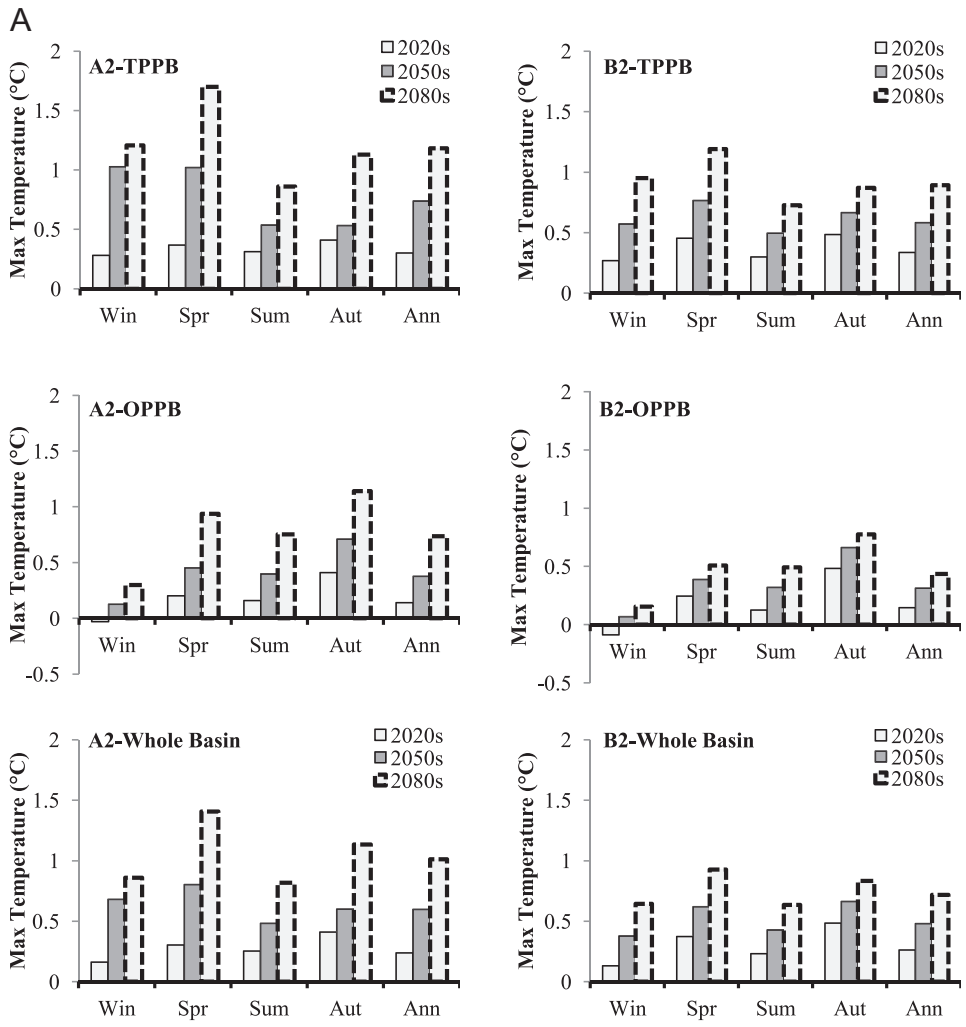

Fig. 6. Future temporal changes in (A) T_{max}, (B) T_{min}, and (C) Precipitation, relative to the baseline period (1961–1990), under A2 and B2 in the TPPB, OPPB, and the whole Jhelum River basin.

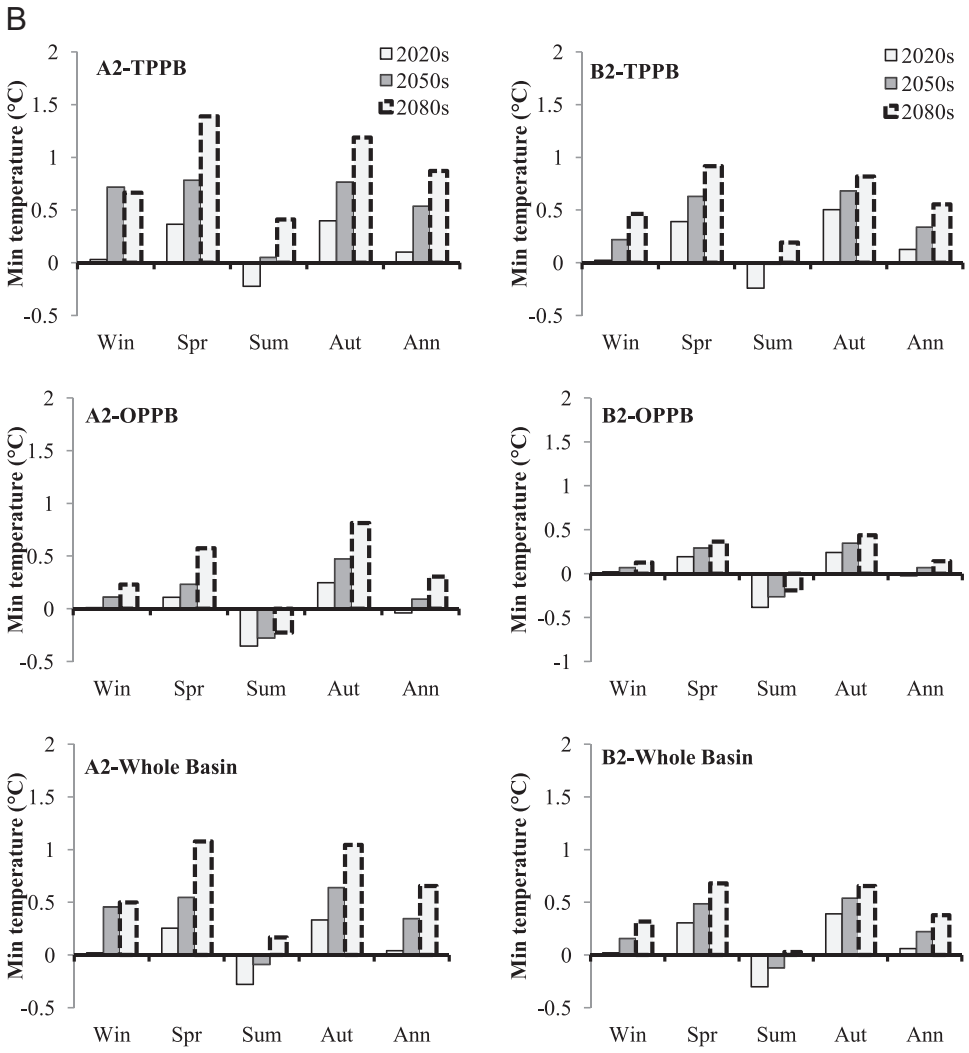

Fig. 6. (*continued*)

For better explanation, the temporal and spatial changes are presented graphically in this paper, as they have also been in other studies (Chu et al., 2010; Huang et al., 2011). Since Gulmarg and Qazigund weather stations lack data starting from 1961, the data for these stations was projected back by SDSM using NCEP predictors.

4. Results and discussion

4.1. Screening of predictors

Table 3 shows the predictors selected after screening, along with their mean absolute partial correlation (P.r) for T_{max}, T_{min}, and P at a significance level of 0.05. It was determined that temperature at 2 m height (*temp*) was a super predictor for Tmax and Tmin in both the OPPB and TPPB sub-basins. A super predictor is the most prominent predictor and it displays maximum correlation with a predictand. For P, surface specific humidity (*shum*) and meridional wind velocity at 500 hPa (*p5_v*) were the most dominant predictors in the TPPB and OPPB respectively, for almost all weather stations. The selected predictors for P also expressed a logical sense because P depends mostly on water vapors (humidity) and wind direction. The selected predictors for the present study also match with the predictors used in several other studies such as Wilby et al. (2002), Chu et al. (2010), Huang et al. (2011), Hashmi et al. (2011), and Mahmood and Babel (2012).

4.2. Calibration of SDSM

The explained variance (E), used as a performance indicator, ranged from 60% to 72% for T_{max}, 67% to 85% for T_{min}, and 8% to 32% for P. The standard error (SE) for T_{max}, T_{min}, and P was 4.6 °C, 3.4 °C, and 0.45 mm/day respectively. These results are satisfactory and comparable with the results of some previous studies like Wilby et al. (2002), Nguyen (2005), Liu et al. (2009), Souvignet and Heinrich (2011), and Huang et al. (2011). In this study, the E values for P were much lower than the E values for T_{max} and T_{min}. Since P is a heterogeneous climate variable and difficult to simulate, the E of P is more likely to be lower than 40%, while the E of temperature is more likely to be greater than 70% (Wilby et al., 2002).

4.3. Validation of SDSM

4.3.1. Tabular

For the validation of SDSM, three datasets were simulated by forcing the NCEP, A2, and B2 predictors, along with their calibrated parameters, for the period of 1991–2000, and for each of the local scale variables (T_{max}, T_{min}, and P). The performance indicators (R, R^2, RMSE, and μ) were calculated using daily, monthly, and

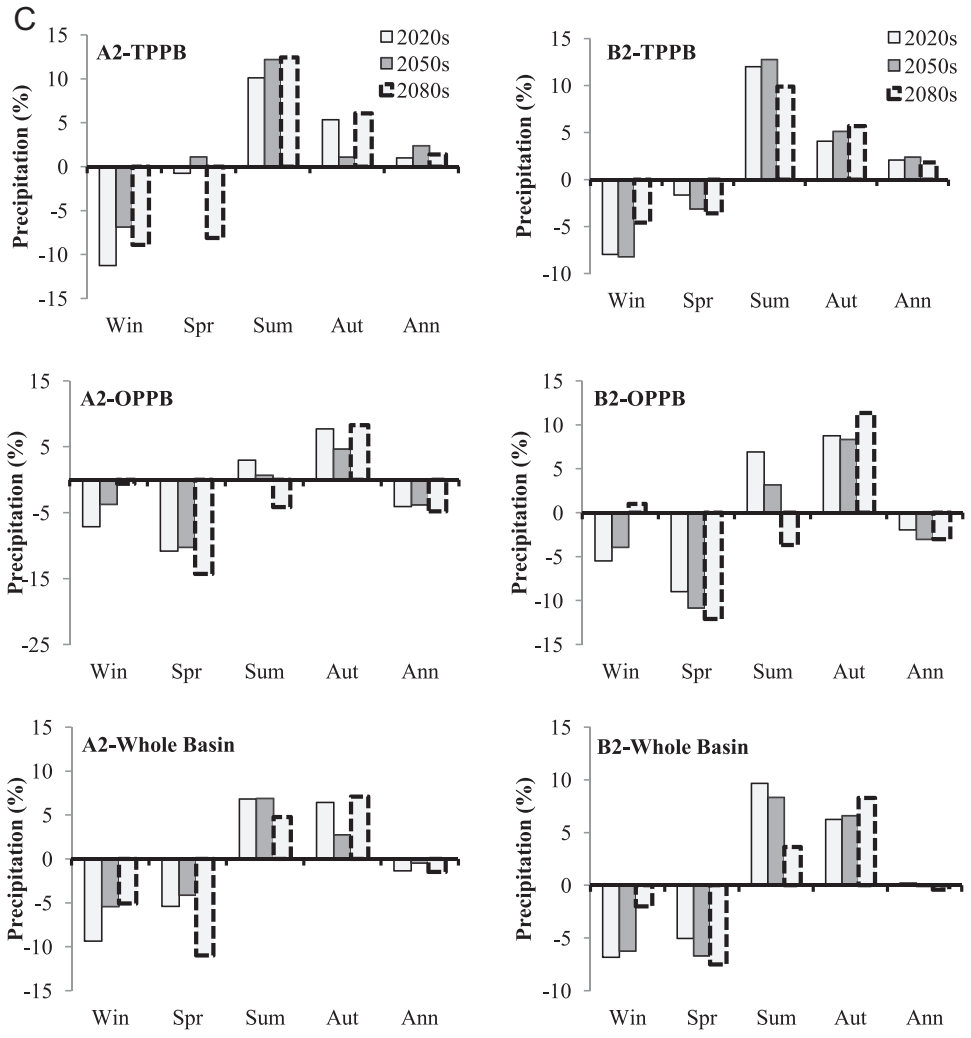

Fig. 6. (*continued*)

seasonal time series from observed and simulated T_{max}, T_{min}, and P. These are described in Tables 4, 5 and 6 respectively.

These tables show that the R^2 values for T_{max} and T_{min} were above 76%, 92% and 94% as calculated from daily, monthly, and seasonal time series respectively. The R^2 values for P were above 9%, 22%, and 50% as calculated from daily, monthly, and seasonal time series respectively. The results of Tmax and Tmin were better than the results of P with respect to all the indicators obtained from the daily, monthly, and seasonal time series, and Tmin results were slightly better than Tmax results. Although the R^2 values obtained by the daily time series (ranging 8–15%) were much lower than those obtained by monthly (21–73%) and seasonal (25–87%) time series when using NCEP predictors, these results are comparable with a previous study (Huang et al., 2011).

The main reason for lower values of R^2 for daily P is the occurrence/amount of P, which is a stochastic process. Therefore, simulation of P is always a difficult task (Huang et al., 2011). Several previous studies (Khan et al., 2006; Fealy and Sweeney, 2007; Huang et al., 2011) have shown worse results obtained from daily time series, compared to results obtained from monthly and seasonal time series. SDSM shows better applicability using monthly and seasonal P time series, relative to the daily time series. It was observed that the results obtained from NCEP predictors were better than A2 and B2 predictors, and the simulated data from A2 gave slightly better results than B2. Since SDSM is calibrated with NCEP predictors, the calibrated parameters reflect some biases when the model is run with A2 and B2 predictors.

4.3.2. Graphical

The main purpose of graphical validation was to investigate the intra-annual variations in the TPPB, OPPB, and in the entire basin, as has been done in several studies (Wilby et al., 2002; Gebremeskel et al., 2005; Zhao and Xu, 2008; Chu et al., 2010; Huang et al., 2011). For this, three datasets for Tmax, Tmin, and P were simulated by forcing the NCEP, A2, and B2 predictors into SDSM and the mean monthly, seasonal, and annual values were calculated and compared with the observed datasets. However, in the present study, only P comparisons are shown graphically in Fig. 4, which illustrates well the intra-annual variations in the TPPB, OPPB, and in the whole basin. The results of T_{max} and T_{min} are not shown graphically in the present study because the results of T_{max} and T_{min} (Tables 4 and 5) were quite satisfactory and much better than P. In addition, P is a heterogeneous variable and it is difficult to capture its variations. Furthermore, it is the most important climate variable among all climate variables

Fig. 4(a) shows that in the TPPB, the big peak occurs in July–August (the monsoon season), and this was reasonably well simulated by all three datasets (NCEP, A2, and B2). On the other hand, the small peak, occurring in March, was underestimated by all three datasets. On the whole, the patterns were well followed by all three data sets.

The mean seasonal precipitations simulated from NCEP and A2 predictors were underestimated and overestimated by 7% and 6% respectively, except in spring (March–May). B2 showed underestimations in winter (December–February) and spring and overestimations in summer (June to August) and autumn (September–November). Overall, B2 underestimated with an average *P* of 0.89%. The mean annual precipitation from NCEP was underestimated by 5.7% and from A2 and B2, it was overestimated by 4% and 1.2% respectively.

Fig. 4(b) indicates that mean monthly *P* was not well simulated by SDSM in the OPPB as it was in the TPPB. Nonetheless, the patterns were followed by all three data sets. The NCEP, A2 and B2 datasets underestimated P in all seasons, with an average seasonal *P* of 6.9%, 11.8%, and 12% respectively, and an average annual P of 6.6%, 13% and 15% respectively.

Fig. 4(c) shows that the big peak was well simulated by all three data sets. However, the small peak was well underestimated by the model. The average seasonal *P*, as simulated by NCEP, A2 and B2, was underestimated by about 6.5%, 2.3% and 6.2% respectively. NCEP, A2, and B2 datasets underestimated the mean annual *P* by 6%, 3.45% and 5.75% respectively.

On the whole, SDSM performed reasonably well in capturing the variations of observed mean monthly, seasonal, and annual *P*. The results from NCEP dataset were better than A2 and B2 because the model was calibrated with NCEP dataset. Nonetheless, results from A2 and B2 datasets were quite comparable with NCEP. These results are also comparable with other studies (Chu et al., 2010; Huang et al., 2011)

4.3.3. Spatial validation

To check the capability of SDSM in simulating spatial changes in the study area, three groups of maps (Fig. 5) for each variable (Tmax, Tmin, and P) were created by converting mean annual point data into raster data with the kriging interpolation method. As can be seen, each group has four maps; one was produced by using observed data and the other three by simulated data—one each from NCEP, A2 and B2 predictors. Two indicator, Absolute Mean Error (AME) and Root Mean Square Standardized Error (RMSSE) were utilized to check the performance of kriging method and results are described in Table 7. AME values for T_{min}, T_{max} and *P* ranged between 0.011 °C and 0.022 °C, 0.018 °C and 0.23 °C, and 7.2 mm and 11.6 mm respectively, in observed, NCEP, A2 and B2 maps, and RMSSE values for T_{min}, T_{max} and *P* were 0.99–1.05, 0.84–0.95, and 1.1–1.2 respectively, which were quite satisfactory.

It was seen that the spatial variations in observed mean annual temperature (T_{max} and T_{min}) and *P* were well reflected by all three downscaled datasets, as is shown by Fig. 5. Spatial distributions of temperature and precipitation showed that temperature decreases from south to north in accordance with the increase in elevation, and *P* decreases from west to east. Spatial variability was reasonably better simulated by NCEP data than by A2 and B2 data, and it was better captured in the TPPB than in the OPPB. Nevertheless, the results from A2 and B2 were comparable with NCEP.

Thus, it was concluded that SDSM is more credible in simulating mean monthly, seasonal and annual future changes in Tmax, Tmin, and P rather than in simulating daily future changes in the Jhelum basin. The calibrated SDSM, with NCEP predictors, can be used to

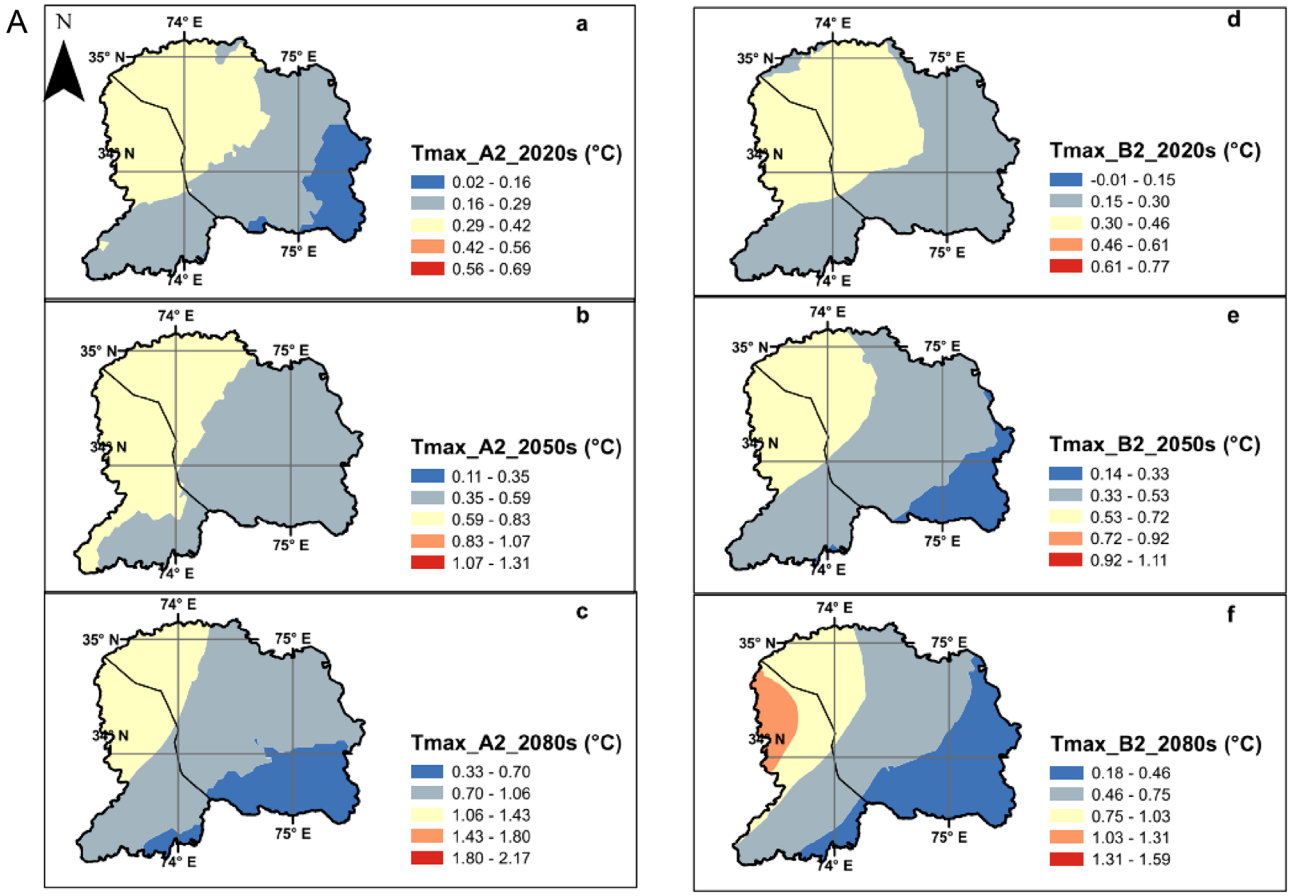

Fig. 7. Future spatial changes in (A) T_{max} (°C), (B) T_{min} (°C), and (C) Precipitation (%) under scenarios A2 and B2, in the Jhelum River basin.

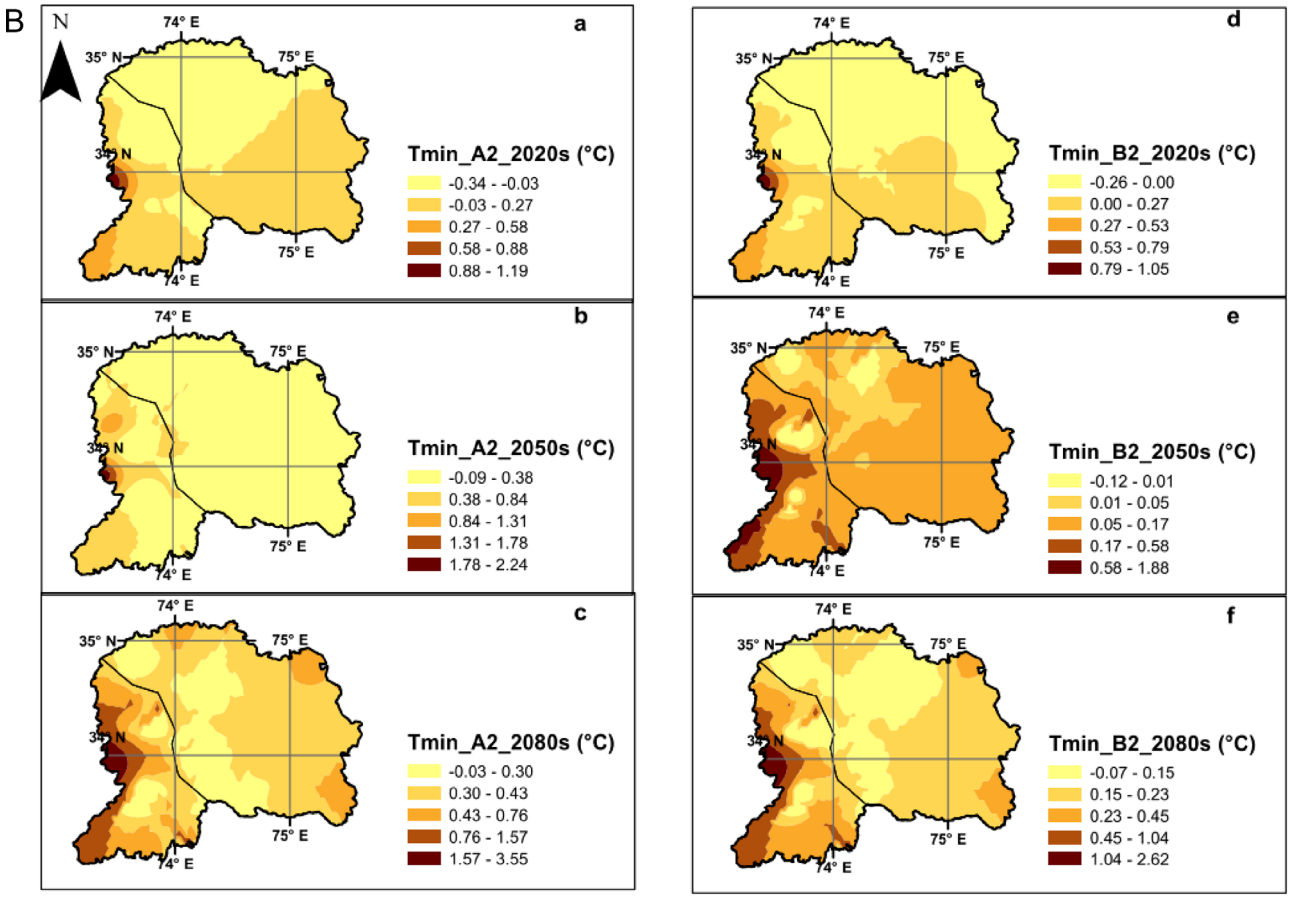

Fig. 7. (*continued*)

predict future changes in T_{max}, T_{min}, and P better with respect to the baseline period, than with A2 and B2 predictors.

5. Temporal and spatial future changes in temperature and precipitation

After successful calibration and validation, daily time series of T_{max}, T_{min}, and P were simulated for the 2020s, 2050s and 2080s using A2 and B2 scenarios. Then, the calculated mean monthly, seasonal and annual T_{max}, T_{min}, and P data from the daily time series was compared with the baseline data to analyze future changes in the 2020s, 2050s and 2080s (Chu et al., 2010; Huang et al., 2011).

5.1. Temporal changes

Fig. 6 (A) shows mean annual and seasonal Tmax changes in the TPPB, OPPB, and in the whole Jhelum basin under A2 and B2 scenarios in the 2020s, 2050s and 2080s. Mean annual T_{max}, under both scenarios, is projected to increase by 0.3–1.2 °C in the TPPB, 0.14–0.74 °C in the OPPB, and 0.24–1.02 °C in the whole Jhelum basin in the 21st century. Kazmi et al. (2015) and Rajbhandari et al. (2015) also showed increasing trends over the whole Pakistan. However, Kazmi et al. (2015) conducted study for the period of 2011–2013 and did not include the whole Jhelum basin because most of the Jhelum basin is situated in Jammu and Kashmir, and Rajbhandari et al. (2015) found out the projected changes over the Indus basin with Regional Climate Model. Similarly, all seasons show positive (increasing) changes under both scenarios in all three future periods (2020s, 2050s, and 2080s) except in winter in the OPPB. Under A2 scenario, in the TPPB and OPPB, the most affected seasons are spring and autumn, with a projected increase of 1.7 °C and 1.14 °C in the 2080s respectively. In the whole basin, spring, with a 1.4 °C increase in the 2080s, shows the most distinct change, relative to the other seasons. The same kinds of future changes are found under B2 but are relatively smaller in magnitude than the changes under A2.

Fig. 6 (B) illustrates the mean annual and seasonal changes in Tmin in the TPPB, OPPB, and in the whole basin under both scenarios in the three future periods. Under both scenarios, mean annual Tmin is predicted to rise by 0.12–0.87 °C in the TPPB, −0.03 to 0.31 °C in the OPPB, and 0.04–0.65 °C in the whole basin. These results are also supported by Kazmi et al. (2015) and Rajbhandari et al. (2015). In the case of seasonal changes, spring is affected more in the TPPB and autumn in the OPPB. The same is also the case of T_{max}. Future changes in T_{min} are predicted to be larger in magnitude under A2 than B2, reflecting the same pattern for Tmax projections.

Fig. 6 (C) presents the percentage changes in mean annual and seasonal P in the TPPB, OPPB, and in the whole basin under both scenarios. Mean annual P is estimated to increase by 1–3% in the TPPB and decrease by 2–5% in the OPPB, under both scenarios, with an overall decrease in the whole basin. As for seasonal changes in the TPPB basin, summer (the monsoon season in the basin) and autumn P show a definite increase of about 1–3% under A2 and 1–6% under B2 in the future, with the exception of the 2080s under B2. In contrast, in the TPPB, winter P is projected to decrease by 7–12% and 5–8% under A2 and B2, respectively. On the whole, in the TPPB, summer and autumn are more likely to receive increased P in the future with respect to the baseline values, and winter as well as spring are likely to receive less P in the future,

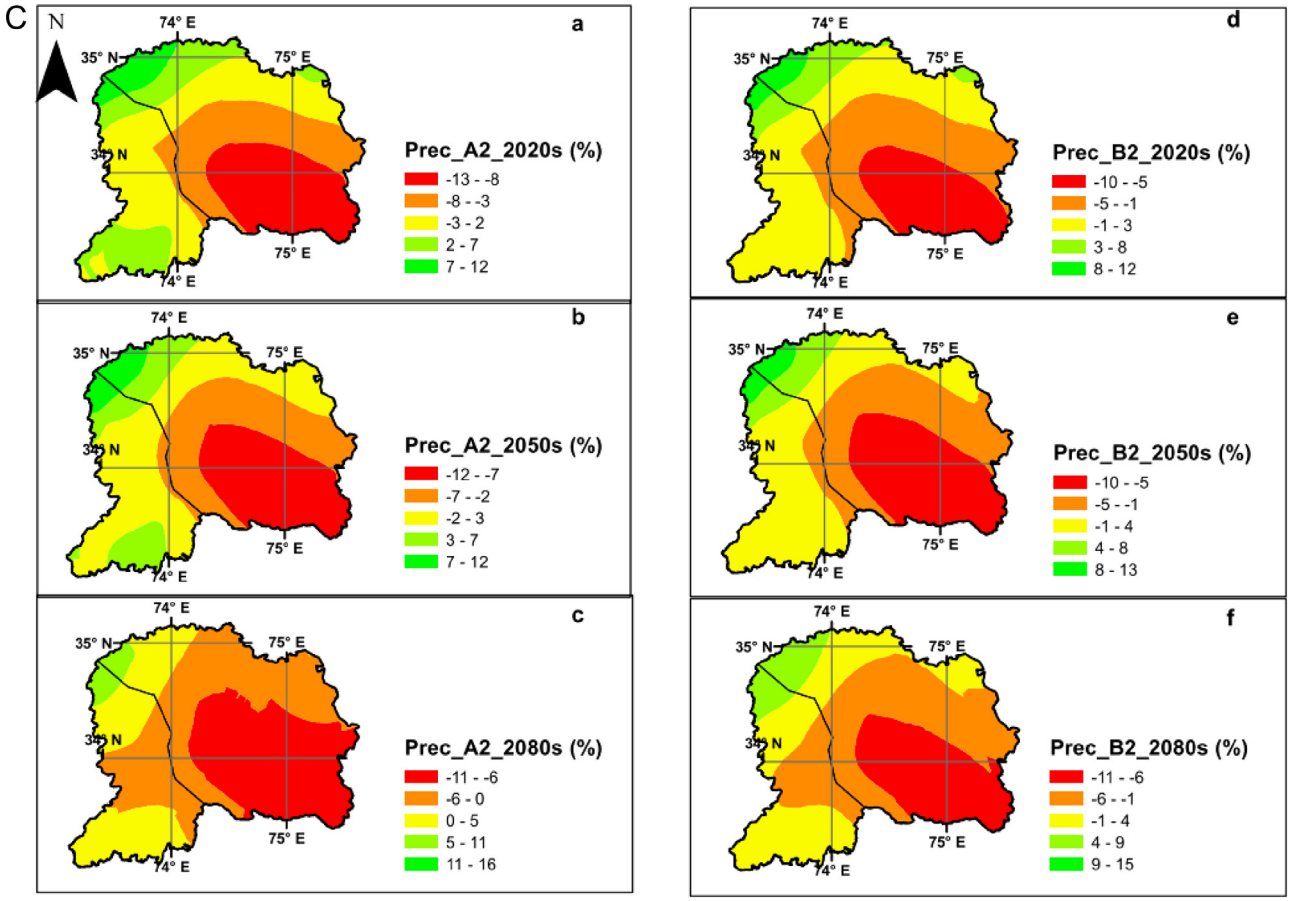

Fig. 7. (*continued*)

Table 8
AME and RMSSE between predicted Tmax, Tmin, and Precipitation for the period of 2020s, 2050s and 2080s, during kriging interpolation, in the Jhelum River basin.

	2020s		2050s		2080s	
T_{min}	A2	B2	A2	B2	A2	B2
AME (°C)	0.0300	0.0100	0.0900	0.0500	0.0120	0.0800
RMSSE	0.9000	0.8611	0.9155	0.9259	0.8750	0.7595
T_{max}						
AME(°C)	0.0200	0.0200	0.0002	0.0200	0.0056	0.0240
RMSSE	1.0043	1.0909	0.9211	0.9333	0.9574	0.9189
Precipitation						
AME(°C)	0.6100	0.4300	0.4500	0.3400	1.2000	0.7800
RMSSE	0.9281	0.9455	0.9400	0.9180	1.0047	0.9644

AME=Absolute Mean Error, *RMSSE*=Root Mean Square Standardized Error

relative to the baseline values. These results are also supported by Rajbhandari et al. (2015). They conducted study for winter and summer monsoon and explored that summer precipitation is projected to increase and winter decrease.

In the OPPB, only autumn presents a definite increase in *P* (by 5–12%) in all three periods under both scenarios. In summer, the changes are positive in the 2020s and 2050s but negative in the 2080s. *P* in spring (the peak season in the OPPB) is projected to decrease by 9–15% under both scenarios.

Therefore, it can be concluded that the peak in the OPPB is likely to go towards dryness in the future. In the whole basin, under both A2 and B2 scenarios, summer and autumn may be wetter than before, and winter and spring may be dryer, as compared to the baseline period. Since most of the meteorological stations are installed in the valleys and not on the high altitudes (on Peaks) and the number of stations available inside the basin is insufficient, as shown in Fig. 1, temperature and precipitation changes in the basin might be different if the high altitudes will be considered.

5.2. Spatial changes

In this study, the mean annual changes in T_{max}, T_{min}, and *P* were also analyzed spatially in the Jhelum River basin under A2 and B2 scenarios, with the help of kriging method, as shown in Fig. 7. The AME and RMSSE between measured and predicted T_{min}, T_{max}, and *P* are presented in Table 8. AME ranged from 0.0002 to 0.09 °C for Temperature (T_{max} and T_{min}) and 0.34 to 1.2 °C, respectively, and RMSSE ranged from 0.74 to 1.004 for Temperature (T_{max} and T_{min}) and 0.92 to 1.005,respectively, under A2 and B2 in 2020s, 2050s and 2080s in the Jhelum River basin.

Fig. 7 (A) shows the spatial distribution of mean annual changes in T_{max} in the 2020s, 2050s and 2080s under A2 and B2 scenarios, relative to the baseline. The northwest part of the basin is projected to be the most affected in all three future periods, with a definite increase in T_{max}. The southeast part of the basin is predicted to be the least affected. T_{max} only shows a small increase in this region. The results also indicate that the changes are mostly increasing moving from southeast to northwest side under both scenarios.

Fig. 7 (B) presents the spatial distribution of mean annual changes in T_{min} in the three future periods under A2 and B2 scenarios, relative to the baseline. Most of the basin shows decrease in T_{min} under A2 in 2020s and 2050s and most of the basin

presents increase in 2080s. Under B2, almost half of the basin gives indication about decrease in T_{min} in 2020s. However, most of the basin shows increase T_{min} in 2050s and 2080s.

Fig. 7 (C) provides the spatial distribution of percentage changes in mean annual P, as compared to the baseline under A2 and B2 scenarios in all three future periods. As can be seen, on the whole, the changes are spread between −13% and 16% over the whole basin under both scenarios, in all three future periods. The simulated decrease in P occurs in eastern part and increases in the west of the basin. It can be seen that almost half of the basin shows decreasing P in the 2020s. However, in the 2080s, it is projected that more than half of the basin will have decreased P under both scenarios. Under both scenarios, similar kinds of spatial distribution patterns of mean annual precipitation changes can be seen, for all three future periods; however, the changes (positive or negative) are higher under A2 than under B2.

6. Conclusions

In this study, a well-known decision support tool, the Statistical Downscaling Model (SDSM), was applied to analyze the temporal and spatial future changes in maximum temperature, minimum temperature and precipitation in the sub-basins, TPPB and OPPB, and in the whole Upper Jhelum River basin under A2 and B2 scenarios. The downscaling of these variables is very important in order to study the impacts of climate change on the hydrological cycle of the basin.

SDSM showed good capability in simulating Tmax and Tmin in daily, monthly, and seasonal time series, during the calibration and validation. However, it presented good results only for monthly and seasonal precipitation. However, only seasonal and annual future changes, with respect to baseline, were presented in this study. Seasonal data was simulated better than monthly and daily data.

Mean annual Tmax and Tmin were projected to increase in both parts of the Jhelum basin, the TPPB and the OPPB, under both scenarios, and in all three future periods. This simulated increase in temperature was higher under A2 than B2 in both the sub-basins and it was higher in the TPPB than OPPB. For seasonal changes in mean annual temperature (Tmax and Tmin), the maximum increase was projected for spring under both scenarios (A2 and B2) in the whole basin. Spring in the TPPB and autumn in the OPPB were projected to be the most affected seasons as far as rise in temperature was concerned.

Mean annual precipitation was predicted to increase by 1–3% in the TPPB and decrease by 2–5% in the OPPB under both scenarios, with an overall decrease in the whole basin. Summer and winter were the most affected seasons in the TPPB under both scenarios and in all three future periods. In the OPPB, autumn showed increase in precipitation, and spring showed decrease under both scenarios. As for the whole basin, summer and autumn were projected to receive more precipitation, and winter as well as spring to receive lesser amounts of precipitation in the future, as compared to baseline period.

The spatial distribution of mean annual T_{max} showed a rise in almost all parts of the basin in the future periods, relative to the baseline period. However, northwestern parts of the basin were projected to face a higher increase than southeastern parts under both scenarios. T_{min} was projected to decrease in some parts of the basin but a majority of the basin will experience a rise in T_{min} under both scenarios especially in 2050s and 2080s, as compared to the baseline values. It was seen that almost half of the basin showed decreasing precipitation in the 2020s, but in the 2080s, decreasing precipitation was likely to be experienced in most parts of the basin under both scenarios. Both scenarios presented similar kinds of spatial distribution patterns of mean annual Tmax, Tmin, and precipitation changes in all three future periods, but with different magnitudes. The changes under A2 were observed higher than under B2.

Acknowledgments

This study is a part of the first author's doctoral research work, conducted at the Asian Institute of Technology Thailand. The authors wish to acknowledge and offer gratitude to Pakistan Meteorological Department (PMD), the Water and Power Development Authority (WAPDA) of Pakistan, the India Meteorological Department (IMD), and the National Climate Data Center (NCDC), for providing important and valuable data for the research. Heartfelt gratitude is also extended to the Higher Education Commission (HEC) of Pakistan and AIT for providing financial support to the first author for his doctoral studies at AIT.

References

Ahmad, I., Ambreen, R., Sun, Z., Deng, W., 2015. Winter-Spring Precipitation Variability in Pakistan. Am. J. Clim. Change 4 (1), 115–139. http://dx.doi.org/10.4236/ajcc.2015.41010.

Ahmad, N., Chaudhry, G.R., 1988. Irrigated agriculture of Pakistan S. Nazir, Lahore.

Akhtar, M., Ahmad, N., Booij, M.J., 2008. The impact of climate change on the water resources of Hindukush–Karakorum–Himalaya region under different glacier coverage scenarios. J. Hydrol. 355 (1-4), 148–163. http://dx.doi.org/10.1016/j.jhydrol.2008.03.015.

Akhtar, M., Ahmad, N., Booij, M.J., 2009. Use of regional climate model simulations as input for hydrological models for the Hindukush-Karakorum-Himalaya region. Hydrol. Earth Syst. Sci. 13 (7), 1075–1089. http://dx.doi.org/10.5194/hess-13-1075-2009.

Anandhi, A., Srinivas, V.V., Nanjundiah, R.S., Nagesh Kumar, D., 2007. Downscaling precipitation to river basin in India for IPCC SRES scenarios using support vector machine. Int. J. Climatol. 28, 401–420. http://dx.doi.org/10.1002/joc.1529.

Archer, D.R., Fowler, H.J., 2008. Using meteorological data to forecast seasonal runoff on the River Jhelum, Pakistan. J. Hydrol. 361 (1-2), 10–23. http://dx.doi.org/10.1016/j.jhydrol.2008.07.017.

Ashiq, M., Zhao, C., Ni, J., Akhtar, M., 2010. GIS-based high-resolution spatial interpolation of precipitation in mountain–plain areas of Upper Pakistan for regional climate change impact studies. Theor. Appl. Climatol. 99 (3), 239–253. http://dx.doi.org/10.1007/s00704-009-0140-y. . http://dx.doi.org/10.1007/s00704-009-0140-y.

Benestad, R.E., Hansen-Bauer, I., Chen, D., 2008. Empirical-statistical Downscaling. World Scientific, New York, p. 215.

Buytaert, W., Celleri, R., Willems, P., Bièvre, B.D., Wyseure, G., 2006. Spatial and temporal rainfall variability in mountainous areas: a case study from the South Ecuadorian Andes. J. Hydrol. 329 (3–4), 413–421. http://dx.doi.org/10.1016/j.jhydrol.2006.02.031.

CCCSN, 2012. Statistical Downscaling Input: HadCM3 Predictors: A2 and B2 Experiments.

Chu, J., Xia, J., Xu, C.Y., Singh, V., 2010. Statistical downscaling of daily mean temperature, pan evaporation and precipitation for climate change scenarios in Haihe River, China. Theor. Appl. Climatol. 99 (1), 149–161. http://dx.doi.org/10.1007/s00704-009-0129-6.

Dai, F., Zhou, Q., Lv, Z., Wang, X., Liu, G., 2014. Spatial prediction of soil organic matter content integrating artificial neural network and ordinary kriging in Tibetan Plateau. Ecol. Indic. 45 (0), 184–194. http://dx.doi.org/10.1016/j.ecolind.2014.04.003.

Diaz-Nieto, J., Wilby, R.L., 2005. A comparison of statistical downscaling and climate change factor methods: impacts on low flows in the River Thames, United Kingdom. Clim. Change 69 (2), 245–268. http://dx.doi.org/10.1007/s10584-005-1157-6.

Fealy, R., Sweeney, J., 2007. Statistical downscaling of precipitation for a selection of sites in Ireland employing a generalised linear modelling approach. Int. J. Climatol. 27 (15), 2083–2094. http://dx.doi.org/10.1002/joc.1506.

Fowler, H.J., Blenkinsop, S., Tebaldi, C., 2007. Linking climate change modelling to impacts studies: recent advances in downscaling techniques for hydrological modelling. Int. J. Climatol. 27 (12), 1547–1578. http://dx.doi.org/10.1002/joc.1556.

Gagnon, S., Singh, B., Rousselle, J., Roy, L., 2005. An application of the statistical downscaling model (SDSM) to simulate climatic data for streamflow modelling in Québec, Canada. Water Resour. J. 30 (4), 297–314. http://dx.doi.org/10.4296/cwrj3004297.

Gebremeskel, S., Liu, Y.B., de Smedt, F., Hoffmann, L., Pfister, L., 2005. Analysing the effect of climate changes on streamflow using statistically downscaled GCM scenarios. Int. J. River Basin Manag. 2 (4), 271–280. http://dx.doi.org/10.1080/15715124.2004.9635237.

Ghosh, S., Mujumdar, P., 2008. Statistical downscaling of GCM simulations to streamflow using relevance vector machine. Water Resour. 31, 132–146.
Goyal, M.K., Ojha, C.S.P., 2010. Robust weighted regression as a downscaling tool in temperature projections. Int. J. Glob. Warm. 2 (3), 234–251. http://dx.doi.org/10.1504/IJGW.2010.036135.
Hashmi, M.Z., Shamseldin, A.Y., Melville, B.W., 2011. Comparison of SDSM and LARS-WG for simulation and downscaling of extreme precipitation events in a watershed. Stoch. Env. Res. Risk A 25 (4), 475–484. http://dx.doi.org/10.1007/s00477-010-0416-x.
Hay, L.E., Clark, M.P., 2003. Use of statistically and dynamically downscaled atmospheric model output for hydrologic simulations in three mountainous basins in the western United States. J. Hydrol. 282 (1–4), 56–75. http://dx.doi.org/10.1016/s0022-1694(03)00252-x.
Hay, L.E., Wilby, R.L., Leavesley, G.H., 2000. A comparison of delta change and downscaled GCM scenarios for three mountainous basins in the United States. J. American Water Resour. Ass. 36 (2), 387–397. http://dx.doi.org/10.1111/j.1752-1688.2000.tb04276.x.
Huang, J., et al., 2011. Estimation of future precipitation change in the Yangtze River basin by using statistical downscaling method. Stoch. Env. Res. Risk A. 25 (6), 781–792. http://dx.doi.org/10.1007/s00477-010-0441-9.
IPCC, 2013. Climate Change 2013: The Physical Science Basis. Contribution of Working Group I to the Fifth Assessment Report of the Intergovern–Mental Panel on Climate Change Cambridge University Press, Cambridge, United Kingdom and New York, NY, USA.
Jacobusse, G., 2005. WinMICE User's manual.
Kazmi, D., et al., 2015. Statistical downscaling and future scenario generation of temperatures for Pakistan Region. Theor. Appl. Climatol. 120 (1–2), 341–350. http://dx.doi.org/10.1007/s00704-014-1176-1.
Khan, M.S., Coulibaly, P., Dibike, Y., 2006. Uncertainty analysis of statistical downscaling methods. J. Hydrol. 319 (1-4), 357–382. http://dx.doi.org/10.1016/j.jhydrol.2005.06.035.
Liu, J., Williams, J.R., Wang, X., Yang, H., 2009. Using MODAWEC to generate daily weather data for the EPIC model. Environ. Model. Softw. 24 (5), 655–664. http://dx.doi.org/10.1016/j.envsoft.2008.10.008.
Mahmood, R., Babel, M., 2012. Evaluation of SDSM developed by annual and monthly sub-models for downscaling temperature and precipitation in the Jhelum basin, Pakistan and India. Theor. Appl. Climatol., 1–18. http://dx.doi.org/10.1007/s00704-012-0765-0.
Mujumdar, P., Ghosh, S., P., 2008. Modeling GCM and scenario uncertainty using a possibilistic approach: application to the Mahanadi River, India. Water Resour. Res. 44, W06407-1.
Nguyen, V., 2005. Downscaling methods for evaluating the impacts of climate change and variability on hydrological regime at basin scale. In: Proceedings of the International Symposium on Role of Water Sciences in Transboundary River Basin Management, Thailand, pp. 1–8.
Opitz-Stapleton, S., Gangopadhyay, S., 2010. A non-parametric, statistical downscaling algorithm applied to the Rohini River Basin, Nepal. Theor. Appl. Climatol. 103 (3–4), 375–386. http://dx.doi.org/10.1007/s00704-010-0301-z.
Pokhrel, R.M., Kuwano, J., Tachibana, S., 2013. A kriging method of interpolation used to map liquefaction potential over alluvial ground. Eng. Geology. 152 (1), 26–37. http://dx.doi.org/10.1016/j.enggeo.2012.10.003.
Qamer, F.M., Saleem, R., Hussain, N., Raza, S.M., 2008. Multi-scale watershed database of Pakistan. In: Proceedings of the 10th International Symposium on High Mountain Remote Sensing Cartography.
Rajbhandari, R., Shrestha, A.B., Kulkarni, A., Patwardhan, S.K., Bajracharya, S.R., 2015. Projected changes in climate over the Indus river basin using a high resolution regional climate model (PRECIS). Clim Dyn. 44 (1-2), 339–357. http://dx.doi.org/10.1007/s00382-014-2183-8.
Souvignet, M., Heinrich, J., 2011. Statistical downscaling in the arid central Andes: uncertainty analysis of multi-model simulated temperature and precipitation. Theor. Appl. Climatol. 106 (1-2), 229–244. http://dx.doi.org/10.1007/s00704-011-0430-z.
Tripathi, S., Srinivas, V.V., Nanjundiah, R.S., 2006. Downscaling of precipitation for climate change scenarios: a support vector machine approach. J. Hydrol. 330 (3–4), 621–640. http://dx.doi.org/10.1016/j.jhydrol.2006.04.030.
Wetterhall, F., Bárdossy, A., Chen, D., S.H., C.-Y, X., 2006. Daily precipitation-downscaling techniques in three Chinese regions. Water Resour. Res. 42, W11423. http://dx.doi.org/10.1029/2005WR004573.
Wilby, R.L., Dawson, C.W., Barrow, E.M., 2002. SDSM — a decision support tool for the assessment of regional climate change impacts. Environ. Model. Softw. 17 (2), 145–157. http://dx.doi.org/10.1016/s1364-8152(01)00060-3.
Wilby, R.L., et al., 2000. Hydrological responses to dynamically and statistically downscaled climate model output. Geophys. Res. Lett. 27 (8), 1199. http://dx.doi.org/10.1029/1999GL006078.
Wilby, R.L., Hay, L.E., Leavesley, G.H., 1999. A comparison of downscaled and raw GCM output: implications for climate change scenarios in the San Juan River basin, Colorado. J. Hydrol. 225 (1–2), 67–91. http://dx.doi.org/10.1016/s0022-1694(99)00136-5.
Wilby, R.L., et al., 2006. Integrated modelling of climate change impacts on water resources and quality in a lowland catchment: River Kennet, UK. J. Hydrol. 330 (1–2), 204–220. http://dx.doi.org/10.1016/j.jhydrol.2006.04.033.
Xu, C.Y., 1999. Climate change and hydrologic models: a review of existing gaps and recent research developments. Water Resour. Manag. 13 (5), 369–382. http://dx.doi.org/10.1023/a:1008190900459.
Zhang, X.C., Liu, W.Z., Li, Z., Chen, J., 2011. Trend and uncertainty analysis of simulated climate change impacts with multiple GCMs and emission scenarios. Agric. For. Meteorol. 151 (10), 1297–1304. http://dx.doi.org/10.1016/j.agrformet.2011.05.010.
Zhao, F.F., Xu, Z.X., 2008. Statistical downscaling of future temperature change in source of the Yellow River Basin. Plateau Meteorol. 27 (1), 153–161 (in Chinese with English abstract).